

Article

Analytical and Numerical Solutions for Three-Dimensional Granular Collapses

Emmanuel Wyser^{1,2,*} , Yury Alkhimenkov^{1,2,3,†} , Michel Jaboyedoff^{1,2,†}  and Yury Y. Podladchikov^{1,2,3,†} ¹ Institute of Earth Sciences, University of Lausanne, 1015 Lausanne, Switzerland² Swiss Geocomputing Centre, University of Lausanne, 1015 Lausanne, Switzerland³ Faculty of Mechanics and Mathematics, Lomonosov Moscow State University, Moscow 119899, Russia

* Correspondence: manuwyser@gmail.com

† These authors contributed equally to this work.

Abstract: This research paper presents a comprehensive approach to investigating dry granular collapses in three dimensions, by combining analytical, numerical, and experimental methods. The experimental investigation utilised a novel apparatus to study granular collapses in the laboratory. It is demonstrated that a quasistatic understanding of granular collapses can accurately predict the final normalised run-out distances for dynamic granular collapses. Our approach involved establishing a correlation between the angle of repose and the initial aspect ratio of the granular column. It is also shown that the material point method (MPM) is suitable for modelling granular collapses in three dimensions. Our in-house solver was further validated using experimental evidence under an explicit formulation, resulting in good agreement between the numerical and experimental results. The findings demonstrate the effectiveness of our in-house solver for three-dimensional granular collapse modelling.

Keywords: granular collapse; GPU computing; generalised interpolation material point method; large deformation



Citation: Wyser, E.; Alkhimenkov, Y.; Jaboyedoff, M.; Podladchikov, Y.Y. Analytical and Numerical Solutions for Three-Dimensional Granular Collapses. *Geosciences* **2023**, *13*, 119. <https://doi.org/10.3390/geosciences13040119>

Academic Editor: Dominic E. L. Ong

Received: 6 March 2023

Revised: 13 April 2023

Accepted: 14 April 2023

Published: 16 April 2023



Copyright: © 2023 by the authors. Licensee MDPI, Basel, Switzerland. This article is an open access article distributed under the terms and conditions of the Creative Commons Attribution (CC BY) license (<https://creativecommons.org/licenses/by/4.0/>).

1. Introduction

The maximum angle above which noncohesive granular material starts to flow is expressed by the angle of repose θ_c [1–3]. This angle is a dominant feature of such material and is stable below the critical angle. The angle varies from 25° for smooth particles to 45° for angular particles [4–6]. Dry sands allow for typical values of approximately 35°, whereas it is much more important under wet conditions with values of approximately 90° or even greater [7]. This angle is related to the friction coefficient μ [8], i.e., $\mu = \tan(\theta_c)$ (see [7] for further details). Other factors that influence the shape of a granular pile include gravity, grain properties (e.g., roughness, sphericity, and grain size [9,10]), the number of particles involved [11–13], and external perturbations such as vibrations that can cause fluidisation, leading to a relaxation stage [3].

The collapse of a dry or wet granular column [14–17] is a well-known problem, for which various experimental and numerical works [18–21] have been conducted. A fundamental metric is the initial aspect ratio of the column $\lambda_0 = h_0/r_0$, where h_0 and r_0 are the initial height and radius of the column, respectively.

The following well-established scaling law [18,22–24] relates λ_0 to $(r_\infty - r_0)/r_0$, i.e.,

$$\frac{r_\infty - r_0}{r_0} = \begin{cases} \alpha \lambda_0 & , \lambda_0 < \lambda_c, \\ \alpha \lambda_0^\gamma & , \lambda_0 \geq \lambda_c, \end{cases} \quad (1)$$

where α and γ are material-dependent coefficients [5,25], λ_c is the initial critical aspect ratio, r_∞ is the final radii of the column, and i.e., is the final run-out distance.

A transition phase exists, according to the initial aspect ratio, i.e., a change from a truncated cone to a cone shape [26]. References [18–20] proposed a power scaling law to $(r_\infty - r_0)/r_0$ for high λ_0 and linear scaling for low λ_0 . Even though such behaviour is often observed in many studies, the value of this transition remains actively discussed.

Reference [27] proposed the following semi-empirical equation to fit their experimental results:

$$\frac{r_\infty}{r_0} = \begin{cases} \frac{1}{2 \tan(\theta_c)} \left(\lambda_0 + \left(4 \tan^2(\theta_c) - \frac{\lambda_0^2}{3} \right)^{1/2} \right) & , \lambda_0 < 0.74, \\ \left(\frac{3\lambda_0}{0.74} \right)^{1/2} & , \lambda_0 \geq 0.74, \end{cases} \quad (2)$$

which implies that $\theta_c = \text{cst.}$ (constant), modulated by the variation of λ_0 . Such a formulation was in agreement with experimental evidence, i.e., a constant final height $h_\infty \approx \min(h_0, r_0 \tan(\phi_y))$, where $\phi_y \approx 36.5^\circ$ is the internal yield angle. We refer to it as a solution to the dynamic deformations of the granular column.

This manuscript proposes an analytical solution to the final run-out distance of the granular continuum, for which we assume quasistatic deformations, i.e., $h_\infty = r_\infty \tan(\theta_c)$, whereas [27] proposed $h_\infty \approx \min(h_0, r_0 \tan(\phi_y))$, i.e., dynamic deformations. These two understandings are summarised in Figure 1. In the case of quasistatic deformations, the granular pile vertically grows in proportion with λ_0 , and we assumed that $\theta_c \approx \phi_y$.

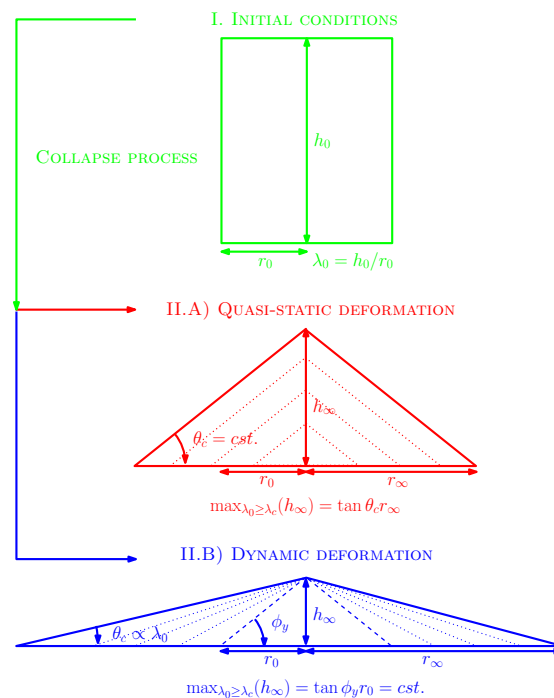


Figure 1. The general scheme of hypothetical quasistatic deformations and the actual experimental evidence of dynamic deformations leading to a constant h_∞ . The dotted lines correspond to increasing volumes with respect to an increasing λ_0 . In Case II B (dynamic deformations), θ'_c naturally decreases as λ_0 increases.

The analytical solution is further compared to: (i) an experimental data collection using a newly designed apparatus and (ii) the reference solution provided by Lajeunesse [27]. The expected differences between the quasistatic solution highlight the characteristic smooth transition between the quasistatic and dynamic deformations of the column. A solution to unify this quasistatic hypothesis with the dynamic understanding of [27] is then provided. Furthermore, the experimental results were compared with three-dimensional numerical

solutions using the material point method (MPM), which is an effective numerical technique for modelling large deformation mechanics [28–31].

2. Materials and Methods

2.1. Laboratory Experiments

2.1.1. Experimental Setup and Data Collection

To eliminate any significant influence from the walls of the container on the flow dynamics of the granular material, a newly designed apparatus is proposed. In previous experiments, the cylinder was rapidly raised upward, resulting in uncontrolled boundary effects at the interface. The proposed experimental setup comprises a cylinder made of three independent shells that quickly open radially outward using a high-performance pneumatic system. This ensures the consistency and reproducibility of the experiments while avoiding any significant influence of the boundaries. The granular material is released and flows freely on a rough wooden surface (see Figure 2). Measurements of the final run-out distance are taken once the column has fully relaxed.

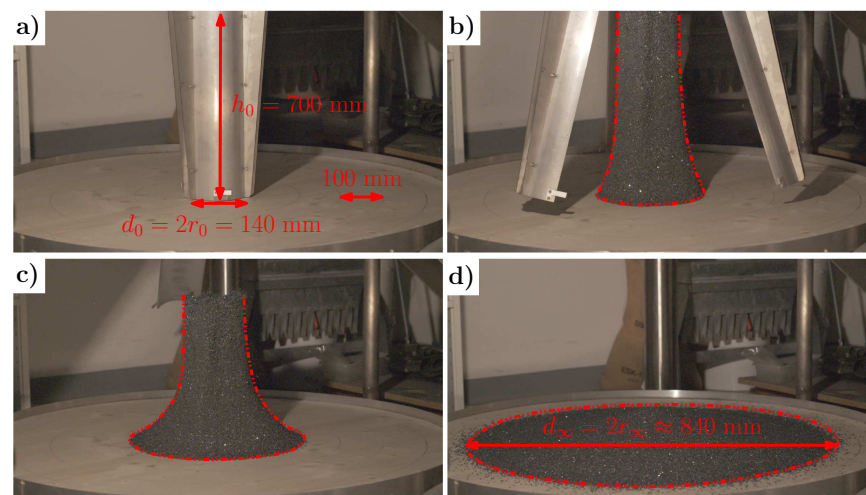


Figure 2. Close-up pictures of the newly designed apparatus used in this study. A cylinder of dimensions 140×700 mm is filled with granular material and (a) quickly opens radially outward from the column's centre, (b) allowing the granular mass to (c) flow freely. The final run-out distance is then measured when (d) the collapse has completely relaxed. The initial aspect ratio is typically $\lambda_0 \leq 10$.

The dense front of the granular mass defines the maximum run-out distance, with measurements taken at six radial locations relative to the centre of the column. The final run-out distance is determined as the average of these six measurements, and individual grain positions are not considered as they are influenced by their previous gaseous state.

The granular mass consists of polydisperse and highly angular silicon carbide beads (SiC) with an average bead diameter of approximately 0.11 cm and a density of $3.21 \text{ g}\cdot\text{cm}^{-3}$. Assuming an equivalent spherical shape, the grain mass is estimated to be 0.02 g. The friction coefficient is relatively high at approximately 0.77, and it was determined by laboratory measurements outlined in the following subsection.

2.1.2. Experimental Estimation of the Angle of Repose θ_c

The angle of repose of the granular material used in this study was measured by slowly raising a vertical cylinder initially filled with the material. The outcome of this process is the formation of a granular pile that is a valid representation of the granular material's quasistatic relaxation. Pictures of the pile were taken using a camera, a CANON EOS 450D, and the procedure was repeated 125 times. The angle of repose over $n = 250$

measurements was determined by processing the pictures and measuring the angles of both sides of the granular pile. Figure 3 shows the simple procedure to determine θ_c .

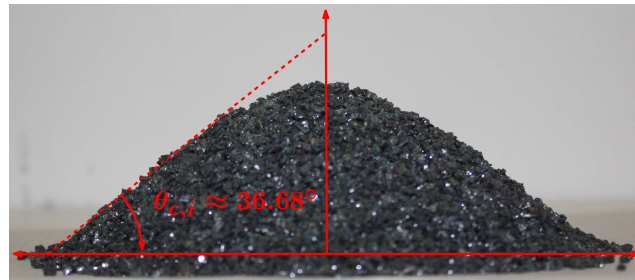


Figure 3. Quasistatic relaxation of a granular material initially contained within a cylinder.

An estimation of the maximal radial distortion was performed using the Agisoft Lens commercial software, and it indicated that the distortion at the edge of the images was approximately 0.18 %, corresponding to a metric distortion of 10^{-4} mm when considering an average sensor distance of $d = 600$ mm. This value was deemed sufficiently low to be negligible.

A cumulated average angle of repose was further calculated and is given by

$$\langle \theta_c \rangle_n = \frac{1}{n} \sum_{i=1}^n \theta_{c,i}, \tag{3}$$

where $n = 250$ measurements (a quantity denoted by the symbol #) of various angles of repose. An average value was identified when an equilibrium was reached, i.e., $\partial_n \langle \theta_c \rangle_n \rightarrow 0$. Figure 4 shows the overall results of the experimental measurements of the angle of repose. This resulted in an average angle of repose $\langle \theta_c \rangle = 37.55^\circ \pm 0.29^\circ$. Using the relation $\mu = \tan(\langle \theta_c \rangle)$, one obtains $\mu \approx 0.77$.

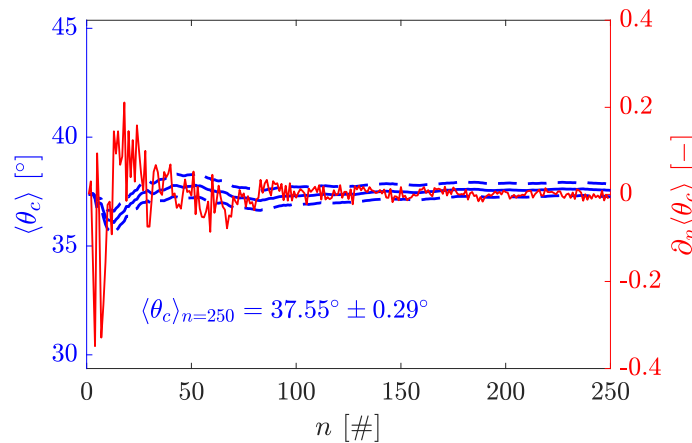


Figure 4. The cumulative average value of the angle of repose is shown by the solid blue line (with the dashed–dotted blue lines indicating the standard deviation of the cumulated average value), and the derivative of the cumulative average value $\langle \theta_c \rangle$ is shown as a function of the number of measurements n .

2.2. A Continuously Smooth Piecewise Analytical Solution

To define a solution $\mathcal{R}(\theta_c, \lambda_0) \equiv (r_\infty - r_0)/r_0$ resulting from the quasistatic relaxation of a granular column as a function of $\tan(\theta_c)$ and λ_0 , let us assume, based on Figure 5, that (i) the mass is conserved and (ii) both the angle of repose θ_c and the initial aspect ratio λ_0 govern the relaxation of the granular column, i.e., a granular pile due to quasistatic deformations during which the internal energy is dissipated by slow frictional interactions only.

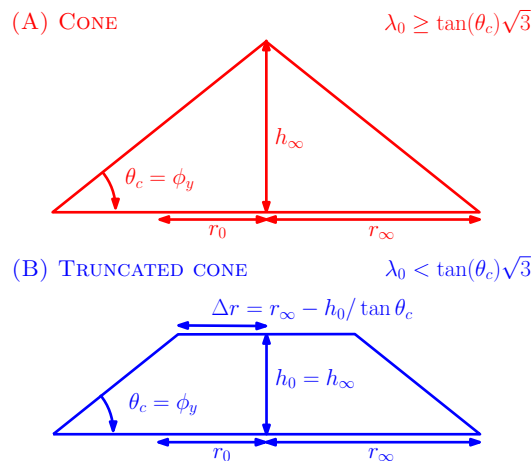


Figure 5. Scheme of the relaxed granular column governed by the angle of repose θ_c and the initial aspect ratio λ_0 under the quasistatic deformation assumption.

The initial volume of the cylinder is given by $V_0 = \pi r_0^2 h_0$, and its final volume is given by $V_\infty = 1/3 \pi r_\infty^2 h_\infty$ (i.e., a cone) or $V_\infty = 1/3 \pi (r_\infty^2 + r_0 \Delta r + \Delta r^2)$ (i.e., a truncated cone). As demonstrated in Figure 5, a transition occurs at $\lambda_c := \tan(\theta_c) \sqrt{3}$, i.e., when $\lambda_0 \rightarrow \lambda_c$.

Considering the relevant dimensions of the problem (Figure 5), the principle of mass conservation dictates that $V_i = V_\infty$, where it is assumed that the granular material is incompressible. The process of equating volumes and substituting and collecting terms results in the following equation:

$$\mathcal{R}(\theta_c, \lambda_0) = \begin{cases} \frac{1}{2} \left(\frac{\lambda_0}{\tan(\theta_c)} + \left(4 - \frac{\lambda_0^2}{3 \tan^2(\theta_c)} \right)^{1/2} \right) - 1 & , \lambda_0 < \tan(\theta_c) \sqrt{3}, \\ \left(\frac{3 \lambda_0}{\tan(\theta_c)} \right)^{1/3} - 1 & , \lambda_0 \geq \tan(\theta_c) \sqrt{3}. \end{cases} \quad (4)$$

This analytical solution assumes quasistatic deformations of the column. To consider the dynamic deformation of the column with a constant final height h_∞ (see Figure 1II B), we relate the angle of repose θ_c to the initial aspect ratio λ_0 , i.e., $\theta_c = f(\lambda_0)$. θ_c is no longer constant, but depends on the initial aspect ratio of the column λ_0 and is given by

$$\theta_c(\lambda_0) = \tan^{-1} \left(\left[\tan^3(\phi_y) / (3 \lambda_0) \right]^{1/2} \right). \quad (5)$$

Inserting Equation (5) within Equation (4) results in a similar formulation with respect to Equation (2) [27].

2.3. Numerical Simulation

The material point method (MPM) was originally proposed by Sulsky (1994) as an extension of the particle-in-cell method. In the MPM, the weak form of the momentum equations is solved on an Eulerian background mesh. Nodal solutions are updated and then mapped to material points, which can be considered as moving Gauss points. The state variables, such as stresses or displacements, are transported by the material points as shown in Figure 6 (taken from [32]). This makes the MPM capable of handling large deformations, such as those occurring in granular flows.

Numerical simulations were conducted to study the three-dimensional dynamics of the granular collapse. The material point method and its variant, the generalised interpolation material point method (GIMP), were employed [33]. An explicit MPM solver that takes advantage of modern graphics processing unit (GPU) architectures was implemented, i.e., ep2-3De v1.0 (The latest version of the solver is available for download from GitHub at: <https://GitHub.com/ewyser/ep2-3De> (last accessed: 10 August 2021).). Further details of the implementation of the solver can be found in [32,34]. Because of the

large deformations involved during the collapse, we selected the uGIMP variant, i.e., the material point's spatial extent is constant (i.e., undeformed; see [35] for the limitations of this variant). A non-associated Drucker–Prager plastic rheology was selected to reproduce the granular collapse [36].

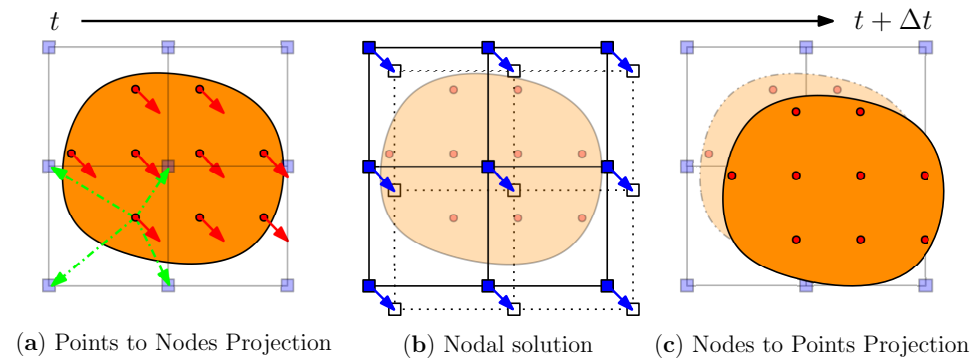


Figure 6. Typical calculation cycle of an MPM solver. (a) The continuum (orange) is discretised by Lagrangian material points (red dots), for which state variables (e.g., mass or stress tensor) are defined.

2.4. Numerical Parameters and Geometry

Recently, Reference [37] demonstrated that density and stiffness properties have a negligible effect on the morphology and run-out distance of granular collapses. Therefore, the same values as [37] were used as we considered the material properties for an effective continuum medium, i.e., a density $\rho = 2000 \text{ kg}\cdot\text{m}^{-3}$, with Young's modulus $E = 5.84 \text{ MPa}$, a cohesion $c = 0 \text{ kPa}$, and a Poisson's ratio $\nu = 0.3$. The friction angle was $\phi = 37.55^\circ$, i.e., $\phi = \langle \theta_c \rangle$, which was measured from our experiments. A local damping D was introduced, for which $D \in [0.05; 0.1]$ is a commonly accepted range for explicit formulations [38]. This local damping is proportional to the magnitude of the out-of-balance forces calculated on the background mesh [38].

Even though GPU programming enables performant (in terms of wall-clock time) numerical solvers and one of the major limitations is the required memory [34], which can far exceed the hardware limit, only one quarter of the granular column was considered, assuming that the horizontal momentum transfers are sufficiently small to be neglected. This allowed an important amount of memory utilisation to be spared on the GPU during computation.

Since the initial aspect ratio λ_0 of the column strongly governs the run-out, we assumed that the numerical geometry could differ from the experimental setting. Consequently, a column of radius $r_0 = 1 \text{ m}$ was considered, to artificially increase the numerical time steps, which are restricted by the Courant–Friedrichs–Lewy (CFL) condition, i.e., adaptive time steps are implemented in `ep2-3De v1.0`. The three-dimensional background mesh is made of regular quadrilateral elements. Roller boundary conditions, i.e., free-slip boundary conditions, were enforced on the side boundaries of the background mesh, whereas a no-slip boundary condition was enforced on the bottom. The granular column was discretised by 40 elements along the x and y directions, and $n_{pe} = 8$ were regularly assigned per the initially filled element (see Table 1). The background mesh depends on the initial height of the column, and it is defined to be sufficiently large to fully enclose the collapse without the influences of side boundaries.

Table 1. The granular column was discretised by 40 elements along the x and y directions, and $n_{pe} = 8$ were assigned per the initially filled element.

λ_0	n_{el}	n_{no}	n_{mp}	Δx [m]
0.5	27,104	30,375	25,120	0.05
1.0	169,344	180,625	50,240	0.05
2.0	1,183,424	1,225,125	100,480	0.05
4.0	8,817,984	8,978,125	200,960	0.05

3. Results

3.1. Analytical Solutions and Experimental Collapses

Figure 7a shows the experimental results from the laboratory experiments fit by: (i) the analytical solution under the quasistatic deformation hypothesis of the column and (ii) the solution given by [27]. The latter agrees with the experimental granular collapses, whereas the former (the present quasistatic understanding of the deformation) rapidly diverges from the experimental data.

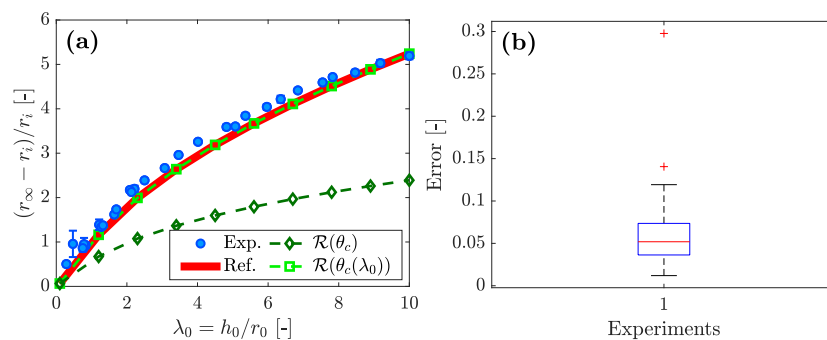


Figure 7. (a) Normalised final run-out distances $(r_\infty - r_0)/r_0$ with respect to the initial aspect ratio $\lambda_0 = h_0/r_0$, with the non-dimensional unit symbol (-). The proposed analytical solution $g(\theta_c)$ (dark green line) predicts lower normalised run-out distances when considering a quasistatic deformation of the column. When relating λ_0 to θ_c , the solution (green line) is in agreement with both the experimental results (blue circles) and the solution proposed by [27] (thick red line). The (b) box plot of the errors for the experimental data demonstrates a rather skewed distribution of errors with a few outliers (red crosses). This explains the overall small amplitude of the error bars in (a).

In this case, $\theta_c = \phi_y$ was considered, where the internal yield angle was $\phi_y = \tan^{-1}(\mu)$ with $\mu = 0.77$. The latter was inferred with the experimental protocol previously presented. When considering $\theta_c = f(\lambda_0)$, the proposed analytical solution (green line in Figure 7a) is then in agreement with both the experimental results and Equation (2) [27].

Regarding the experimental data, a small amplitude of the error measurements was observed (see Figure 7b). This indicates that the present observations are consistent and reliable.

To quantify the goodness of fit of Equation (4), a power-law fit was applied to the experimental data. It is given by

$$\frac{(r_\infty - r_0)}{r_0} = 0.63\lambda_0^{1.30}, \tag{6}$$

for which the root-mean-squared error $RMSE = 0.13$ ($R^2 = 0.99$), which is lower than the proposed analytical solution. An $RMSE = 0.23$ was obtained for $\phi_y = \tan^{-1}(\mu)$. The optimal ϕ_y was further investigated (see Figure 8) for which the $RMSE$ for Equation (4) was the smallest when fit to the experimental data.

The difference observed for the parameter μ (i.e., 0.71 and 0.77 according to Figure 8) appears reasonable. The value inferred from the robust fitting showed the smallest $RMSE$; however, the value inferred from the laboratory measurements has a physical meaning (i.e.,

the friction) despite its greater error. Since the error difference is acceptable, we considered $\mu = 0.77$.

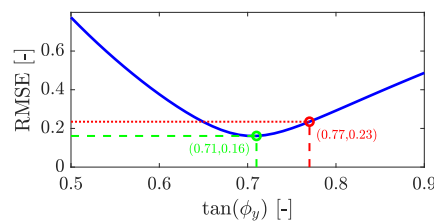


Figure 8. Optimisation of the parameter $\mu = \tan(\phi_y)$. The smallest RMSE is resolved for $\mu = 0.71$, whereas the physical value $\mu = 0.77$, derived from laboratory measurements, is similar in magnitude. However, such an RMSE value is still greater than the one obtained by robust power-law fitting.

3.2. Experimental and Numerical Granular Collapses

A typical numerical solution obtained with the uGIMP variant in ep2-3De v1.0 (see [34]) is shown in Figure 9. The initial aspect ratio was $\lambda_0 = 2$, and the local damping was $D = 0.05$. The granular mass spread in a realistic fashion on the bottom surface. The equivalent plastic strain ϵ_{eqv}^p highlighted intense zones of shearing. However, successive shear bands were roughly resolved because of the numerical resolution, i.e., $\Delta x = 0.05$ m. One can observe that most of the plastic deformation was superficial. In addition to the overall elastoplastic deformations of the granular column, shallower granular avalanches also occurred. Few material points can be considered fully disconnected from the main body, i.e., the gaseous state observed during the experiments. Similarly, the proportion of material points in a disconnected state increased as the local damping was reduced.

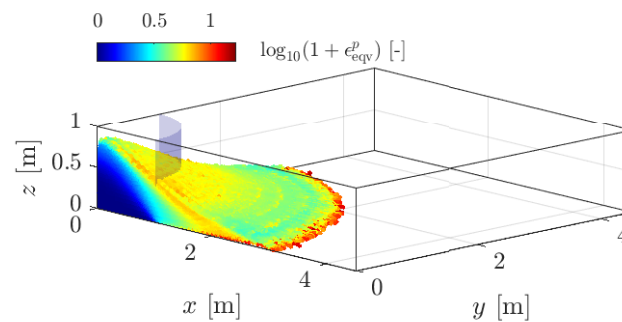


Figure 9. Final morphology of the granular deposit for $\lambda_0 = 2$ and $D = 0.05$. The colour denotes the equivalent plastic strain $\epsilon_{eqv}^p = \int_{t_0}^t (\frac{2}{3} \dot{\epsilon}^p : \dot{\epsilon}^p)^{\frac{1}{2}} dt$ with the plastic strain rate tensor $\dot{\epsilon}^p$, the symbol : denotes the inner product operator. The transparent blue shell indicates the initial maximum extent of the granular column.

Different values were selected for the local damping, i.e., $D = \{0.0, 0.05, 0.1\}$ (see Appendix A for further details). For simplicity, the maximal radial distance of the farthest material point is reported to determine r_∞ . For $D = 0.05$ (see Figure 10), the numerical solution agreed well with the experimental granular collapses. If the damping was smaller or greater than 0.05, the numerical model either overestimated or underestimated the normalised run-out distance, respectively. As such, local damping is an important parameter and requires an iterative calibration process.

Increasing the local damping even more (i.e., $D = 0.4$) led to a numerical solution closer to the proposed analytical solution assuming quasistatic deformation. This makes sense since most of the out-of-balance forces were damped out during the calculation, yielding final run-out distances close to the quasistatic state assumed previously.

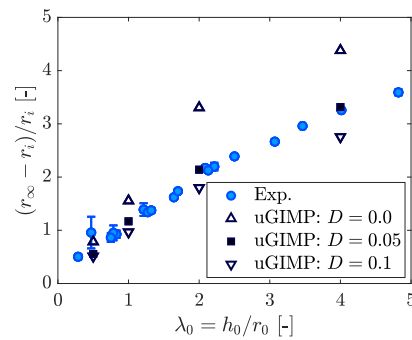


Figure 10. Direct comparison between the experimental results and the numerical solutions using ep2-3De v1.0. The local damping D strongly influences the final normalised run-out distance. This was expected since it damps the out-of-balance forces calculated on the background mesh. For $D = 0.05$, the numerical solution given by ep2-3De v1.0 agrees with the experiments, even though some discrepancies exist.

4. Discussion

The difference between the present analytical solutions (quasistatic and dynamic hypotheses; see Figure 11) expresses an important principle under the following hypothesis. The kinetic energy loss nearly asymptotically increased during the collapse because of an increase in the elastoplastic collision rate. This suggested that the final angle of repose θ_c of a granular collapse expresses the amount of energy lost during the process, compared to a purely quasistatic deformation of the column: the greater the difference between θ_c and ϕ_y , the greater the kinetic energy loss is.

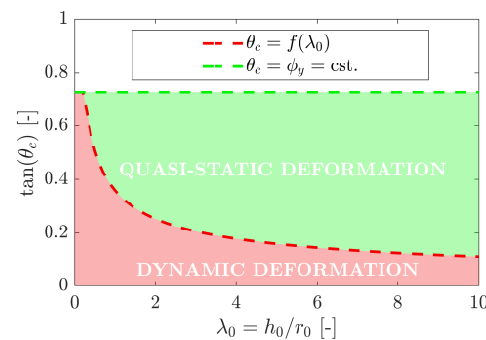


Figure 11. Difference between quasistatic (sand pile, green area) and dynamic deformations (collapse, red area) of the granular column: $\tan(\theta_c)$ expresses the ratio h_∞/r_∞ and shows a significant decrease when $\theta_c = f(\lambda_0)$. It also indirectly expresses the increase in energy loss due to elastoplastic collisions during the inertial deformation of the continuum.

Further interpretation yielded the following. The near-asymptotic behaviour of $\tan(\theta_c)$ (see Figure 11) could be understood because of a microscopic steady-state collision rate during the granular collapse. The collision rate rapidly increased as the initial aspect ratio increased. When the grains reached their free-fall velocity, their collision rate became steady. When such an equilibrium is resolved, the energy dissipation rate within the system can no longer change.

Within the MPM framework under an explicit formulation, the numerical solutions agreed with the experimental results of granular collapses. This confirmed the solver ep2-3De v1.0 to be an appropriate tool for the numerical modelling of dynamic granular collapses. However, a proper calibration procedure for local damping must be conducted. An increase of the local damping yielded a numerical solution closer to the quasistatic analytical solution. However, the explicit formulation of the solver is not well suited to further investigate such numerical transitions. An implicit formulation [39,40] should be preferred to fully resolve quasistatic granular collapses.

Because of hardware limitations (e.g., on-chip memory limit), a full three-dimensional model of granular collapse is not yet possible. This should be the focus of future studies by proposing a multi-GPU implementation of the solver `ep2-3De v1.0` using a message-passing interface standard (MPI), such as Open MPI.

As suggested by [37], some material properties (i.e., stiffness and density) had little influence on the behaviour of the collapse. The only common material parameter between the experiments and the numerical model was the friction angle. Nevertheless, the numerical solutions agreed well with the experimental data. This also demonstrated that the only geometrical parameter that truly matters was the initial aspect ratio λ_0 of the column.

5. Conclusions

We proposed an analytical solution for the normalised run-out distance of three-dimensional quasistatic granular collapses. We further introduced a correction to consider dynamic collapses and the influence of the initial aspect ratio λ_0 of the column as a modulation of the angle of repose θ_c . Such an analytical solution was found to be in good agreement with the experimental results. This demonstrated that a quasistatic understanding of granular collapses can include its dynamic counterpart as well by including a relation between the final angle of repose with the initial aspect ratio of the column. Here, we can only further assume that energy dissipation during the collapse plays a key role in determining the final angle of repose. This may explain the observed variations in the final angle of repose.

Furthermore, we validated our proprietary explicit solver, `ep2-3De v1.0`, by comparing it with experimental granular collapses. Our results demonstrated good agreement and revealed that the introduction of a damping factor modulation enabled us to simulate both quasistatic and dynamic granular collapses. This also allowed us to establish a calibration procedure to determine the optimal damping parameter for use within an explicit material point framework. Taken together, these findings provide strong evidence for the accuracy of our solver in resolving granular collapses. However, future work should focus on two important directions: (1) implementing a multi-GPU approach to overcome the limitations of on-chip memory and (2) developing an implicit formulation of the solver that can natively resolve quasistatic granular collapses and facilitate comparisons with damped explicit solutions.

To improve the robustness and applicability of the proposed analytical solution, future experimental investigations should explore the effects of various shapes of grains. Investigating the impact of irregular grain shapes on the validity of the proposed analytical solutions would be particularly interesting. This objective could be accomplished through the use of different types of granular materials, e.g., long and elongated grains such as rice or quite spherical beads.

Author Contributions: Conceptualisation, M.J. and Y.Y.P.; methodology, E.W.; software, E.W. and Y.A.; validation, E.W.; writing—original draft preparation, E.W. and Y.A.; writing—review and editing, E.W. and Y.A.; supervision, M.J. and Y.Y.P. All authors have read and agreed to the published version of the manuscript.

Funding: This research was supported by the Swiss National Science Foundation (Grant No. 172691) and the Russian Ministry of Science and Higher Education (Project No. 075-15-2022-1106).

Data Availability Statement: Not applicable.

Acknowledgments: Yury Alkhimenkov gratefully acknowledges support from the Swiss National Science Foundation (Grant No. 172691). Yury Alkhimenkov and Yury Y. Podladchikov gratefully acknowledge support from the Russian Ministry of Science and Higher Education (Project No. 075-15-2022-1106).

Conflicts of Interest: The authors declare no conflict of interest.

Sample Availability: The solver ep2-3De v1.0 used in this study is licensed under the GPLv3 free software license. The solver ep2-3De v1.0 archive (v1.0) is available from a permanent DOI repository (Zenodo) at <https://doi.org/10.5281/zenodo.5600373> (the latest version of the code is available for download from GitHub at <https://GitHub.com/ewyser/ep2-3De>, last access: 26 October 2021).

Abbreviations

The following abbreviations are used in this manuscript:

MPM	Material point method
GIMP	Generalised interpolation material point method
GPU	Graphics processing unit
MPI	Message-passing interface

Appendix A

We present the Supplementary Materials regarding the transition from dynamic to quasistatic granular collapses. We report the influence of local damping (see Figure A1) on the behaviour of the granular collapse, i.e., an increase in damping yields a more pronounced quasistatic deformation of the granular column. We selected different values for the local damping, i.e., $D = \{0.0, 0.05, 0.1, 0.2, 0.4\}$.

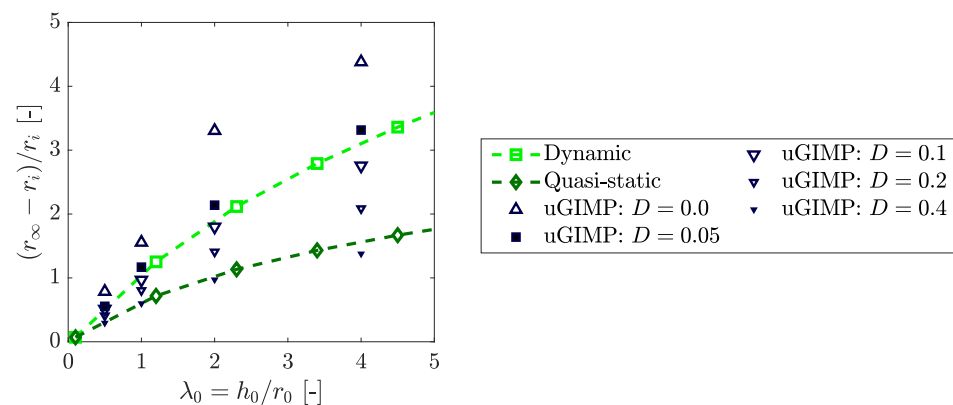


Figure A1. Normalised run-out distances with respect to an initial aspect ratio of column λ_0 for a variety of local damping coefficients D . Analytical solutions under quasistatic and dynamic hypotheses are also reported.

We observed that, as the local damping coefficient increased, the numerical solution came closer to the quasistatic analytical solution we proposed. For $D = 0.4$, the numerical solution was the closest to a quasistatic relaxation of the granular column.

References

1. Lowe, D.R. Grain flow and grain flow deposits. *J. Sediment. Res.* **1976**, *46*, 188–199.
2. Barabási, A.L.; Albert, R.; Schiffer, P. The physics of sand castles: Maximum angle of stability in wet and dry granular media. *Phys. A Stat. Mech. Its Appl.* **1999**, *266*, 366–371. [CrossRef]
3. Tsuji, D.; Otsuki, M.; Katsuragi, H. Relaxation dynamics of a granular pile on a vertically vibrating plate. *Phys. Rev. Lett.* **2018**, *120*, 128001. [CrossRef]
4. Carrigy, M.A. Experiments on the angles of repose of granular materials 1. *Sedimentology* **1970**, *14*, 147–158. [CrossRef]
5. Balmforth, N.J.; Kerswell, R.R. Granular collapse in two dimensions. *J. Fluid Mech.* **2005**, *538*, 399–428. [CrossRef]
6. Pohlman, N.A.; Severson, B.L.; Ottino, J.M.; Lueptow, R.M. Surface roughness effects in granular matter: Influence on angle of repose and the absence of segregation. *Phys. Rev. E* **2006**, *73*, 031304. [CrossRef]
7. Mitarai, N.; Nori, F. Wet granular materials. *Adv. Phys.* **2006**, *55*, 1–45. [CrossRef]
8. Lee, J.; Herrmann, H.J. Angle of repose and angle of marginal stability: Molecular dynamics of granular particles. *J. Phys. A Math. Gen.* **1993**, *26*, 373–383. [CrossRef]
9. Miller, R.L.; Byrne, R.J. The angle of repose for a single grain on a fixed rough bed. *Sedimentology* **1966**, *6*, 303–314. [CrossRef]
10. Buffington, J.M.; Dietrich, W.E.; Kirchner, J.W. Friction angle measurements on a naturally formed gravel streambed: Implications for critical boundary shear stress. *Water Resour. Res.* **1992**, *28*, 411–425. [CrossRef]

11. Grasselli, Y.; Herrmann, H.J.; Oron, G.; Zapperi, S. Effect of impact energy on the shape of granular heaps. *Granul. Matter* **2000**, *2*, 97–100. [CrossRef]
12. Kleinhans, M.G.; Markies, H.; de Vet, S.J.; in't Veld, A.C.; Postema, F.N. Static and dynamic angles of repose in loose granular materials under reduced gravity. *J. Geophys. Res. Planets* **2011**, *116*. Available online: <https://agupubs.onlinelibrary.wiley.com/doi/pdf/10.1029/2011JE003865> (accessed on 3 March 2018). [CrossRef]
13. Al-Hashemi, H.M.B.; Al-Amoudi, O.S.B. A review on the angle of repose of granular materials. *Powder Technol.* **2018**, *330*, 397–417. [CrossRef]
14. Mangeney, A.; Roche, O.; Hungr, O.; Mangold, N.; Faccanoni, G.; Lucas, A. Erosion and mobility in granular collapse over sloping beds. *J. Geophys. Res. Earth Surf.* **2010**, *115*, F03040. [CrossRef]
15. Rondon, L.; Pouliquen, O.; Aussillous, P. Granular collapse in a fluid: Role of the initial volume fraction. *Phys. Fluids* **2011**, *23*, 073301. [CrossRef]
16. Kumar, K.; Delenne, J.Y.; Soga, K. Mechanics of granular column collapse in fluid at varying slope angles. *J. Hydrodyn.* **2017**, *29*, 529–541. [CrossRef]
17. Bougouin, A.; Lacaze, L. Granular collapse in a fluid: Different flow regimes for an initially dense-packing. *Phys. Rev. Fluids* **2018**, *3*, 064305. [CrossRef]
18. Staron, L.; Hinch, E.J. Study of the collapse of granular columns using two-dimensional discrete-grain simulation. *J. Fluid Mech.* **2005**, *545*, 1–27. [CrossRef]
19. Lube, G.; Huppert, H.E.; Sparks, R.S.J.; Freundt, A. Collapses of two-dimensional granular columns. *Phys. Rev. E* **2005**, *72*, 041301. [CrossRef]
20. Lagrée, P.Y.; Staron, L.; Popinet, S. The granular column collapse as a continuum: Validity of a two-dimensional Navier-Stokes model with a $\mu(I)$ -rheology. *J. Fluid Mech.* **2011**, *686*, 378. [CrossRef]
21. Dunatunga, S.; Kamrin, K. Continuum modelling and simulation of granular flows through their many phases. *J. Fluid Mech.* **2015**, *779*, 483–513. [CrossRef]
22. Thompson, E.L.; Huppert, H.E. Granular column collapses: Further experimental results. *J. Fluid Mech.* **2007**, *575*, 177. [CrossRef]
23. Warnett, J.; Denissenko, P.; Thomas, P.; Kiraci, E.; Williams, M. Scalings of axisymmetric granular column collapse. *Granul. Matter* **2014**, *16*, 115–124. [CrossRef]
24. Langlois, V.J.; Quiquerez, A.; Allemand, P. Collapse of a two-dimensional brittle granular column: Implications for understanding dynamic rock fragmentation in a landslide. *J. Geophys. Res. Earth Surf.* **2015**, *120*, 1866–1880. [CrossRef]
25. Mériaux, C. Two dimensional fall of granular columns controlled by slow horizontal withdrawal of a retaining wall. *Phys. Fluids* **2006**, *18*, 093301. [CrossRef]
26. Lo Giudice, A.; Giammanco, G.; Fransos, D.; Preziosi, L. Modeling sand slides by a mechanics-based degenerate parabolic equation. *Math. Mech. Solids* **2019**, *24*, 2558–2575. [CrossRef]
27. Lajeunesse, E.; Mangeney-Castelnau, A.; Vilotte, J. Spreading of a granular mass on a horizontal plane. *Phys. Fluids* **2004**, *16*, 2371–2381. [CrossRef]
28. Baumgarten, A.S.; Kamrin, K. A general fluid–sediment mixture model and constitutive theory validated in many flow regimes. *J. Fluid Mech.* **2019**, *861*, 721–764. [CrossRef]
29. Fern, J.; Rohe, A.; Soga, K.; Alonso, E. *The Material Point Method for Geotechnical Engineering: A Practical Guide*; CRC Press: Boca Raton, FL, USA, 2019.
30. Fern, E.J.; Soga, K. The role of constitutive models in MPM simulations of granular column collapses. *Acta Geotech.* **2016**, *11*, 659–678. [CrossRef]
31. Soga, K.; Alonso, E.; Yerro, A.; Kumar, K.; Bandara, S. Trends in large-deformation analysis of landslide mass movements with particular emphasis on the material point method. *Géotechnique* **2016**, *66*, 248–273. [CrossRef]
32. Wyser, E.; Alkhimenkov, Y.; Jaboyedoff, M.; Podladchikov, Y.Y. A fast and efficient MATLAB-based MPM solver: fMPMM-solver v1.1. *Geosci. Model Dev.* **2020**, *13*, 6265–6284. [CrossRef]
33. Bardenhagen, S.G.; Kober, E.M. The generalized interpolation material point method. *Comput. Model. Eng. Sci.* **2004**, *5*, 477–496.
34. Wyser, E.; Alkhimenkov, Y.; Jaboyedoff, M.; Podladchikov, Y.Y. An explicit GPU-based material point method solver for elastoplastic problems (ep2-3De v1.0). *Geosci. Model Dev.* **2021**, *14*, 7749–7774. [CrossRef]
35. Coombs, W.; Augarde, C.; Brennan, A.; Brown, M.; Charlton, T.; Knappett, J.; Motlagh, Y.; Wang, L. On Lagrangian mechanics and the implicit material point method for large deformation elasto-plasticity. *Comput. Methods Appl. Mech. Eng.* **2020**, *358*, 112622. [CrossRef]
36. Huang, P.; Li, S.I.; Guo, H.; Hao, Z.M. Large deformation failure analysis of the soil slope based on the material point method. *Comput. Geosci.* **2015**, *19*, 951–963. [CrossRef]
37. Nguyen, N.H.T.; Bui, H.H.; Nguyen, G.D. Effects of material properties on the mobility of granular flow. *Granul. Matter* **2020**, *22*, 59. [CrossRef]
38. Wang, B.; Vardon, P.; Hicks, M. Investigation of retrogressive and progressive slope failure mechanisms using the material point method. *Comput. Geotech.* **2016**, *78*, 88–98. [CrossRef]

39. Charlton, T.J.; Coombs, W.M.; Augarde, C.E. iGIMP: An implicit generalised interpolation material point method for large deformations. *Comput. Struct.* **2017**, *190*, 108–125. . [[CrossRef](#)]
40. Coombs, W.M.; Augarde, C.E. AMPLE: A Material Point Learning Environment. *Adv. Eng. Softw.* **2020**, *139*, 102748. . [[CrossRef](#)]

Disclaimer/Publisher's Note: The statements, opinions and data contained in all publications are solely those of the individual author(s) and contributor(s) and not of MDPI and/or the editor(s). MDPI and/or the editor(s) disclaim responsibility for any injury to people or property resulting from any ideas, methods, instructions or products referred to in the content.